Stress-oriented 3D printing path optimization based on image processing algorithms for reinforced load-bearing parts

Yingguang Li [a], Ke Xu [a], Xu Liu [b], Mengyuan Yang [a], James Gao [c], Paul Maropoulos [d]

a College of Mechanical and Electrical Engineering, Nanjing University of Aeronautics and Astronautics, Nanjing 210016, China
b School of Mechanical and Power Engineering, Nanjing University of Technology, Nanjing 211816, China
c School of Engineering, University of Greenwich, Chatham Maritime, Kent ME4 4TB, UK
d School of Mechanical and Aerospace Engineering, Queen's University Belfast, Belfast, BT7 1NN, UK

Abstract:
Fibre reinforced filament fabrication is a potential additive manufacturing method for certain load-bearing parts in aerospace and automotive products. In current practice, printing paths are planned from part geometry without considering loading conditions. This paper presents a new method for optimizing printing paths to align with the principal stress field of parts in use. Because of the powerful processing capabilities, for the first time grayscale image was adopted to represent the irregular vector field, which can be robustly processed into sub-regions for generating regular printing paths. Preliminary bending test achieved promising increase in tensile strength compared with conventional methods

Keywords: Additive manufacturing, Tool path, Image processing

1. Introduction

Fibre reinforced plastics (FRP) filaments have the potential to be used for 3D printing of load-bearing parts in aerospace and automotive industries [1]. The tensile strength of fabricated FRP parts can be 200% higher than those traditionally formed by polylactic acid (PLA) [2], with competitive strength and modulus to those of compression molded parts [3]. Previous research reported high level anisotropy in tensile capacity of the filament fabricated parts due to the great discrepancy of strength along and across the filament [4]. Based on Michell's theory [5], the mechanical strength of printed parts can be maximized if printing paths are aligned with the principal stress directions induced by external loading. Such principal direction can be determined in advance to guide the actual process. According to reported experiments, the tensile and compressive strengths of parts were enhanced by 176% and 21% respectively when printing paths were aligned with principal directions, compared with printing paths in perpendicular direction [6], highlighting the importance of filament layout optimization to fortify the functional performance of parts under external loading conditions.

The layout of filament, i.e., the printing paths, are carefully planned and evaluated to align with principal directions before the printing process [7, 8]. Unlike commercial 3D printing systems that attempt to achieve quasi-isotropic property for fabricated parts, previous researchers proposed various path planning algorithms to enhance the load-bearing capacity of 3D printed parts using both ordinary and fibre reinforced plastics, and achieved noticeable improvements. Steuben et al. [9] applied von Mises stress field to generate level-set infill paths, which were however not evenly spaced due to the irregularity of the stress field. Tam and Mueller [10] proposed stress aligning additive manufacturing for 2-manifold structure

using a robotic arm. Zhang et al. [11] conducted a study on the performance gain of printed carbon fibre reinforced polymer composites by slightly changing the printing path to reduce stress concentration. A greedy tracing algorithm was proposed [12] to enhance the mechanical properties by following the load transmission path when printing FRP. Sun et al. [13] delivered a bioinspired parallel-scan path to increase fracture deflection by incrementally changing the path direction upon each layer. Fang et al. [6] proposed reinforced fused deposition modeling for multi-axis printing of freeform parts, and achieved increased load-bearing performance.

Albeit previous methods achieved promising advances in strengthening 3D printed parts, there are still certain limitations to be solved. In particular, previous methods showed that aligning the filament along the principal direction was effective to improve mechanical strength of respective local area, however could possibly lead to uneven material deposition with voids and overlaps in between two neighboring filaments, which nonetheless could undermine the overall mechanical behavior. Essentially, there was a trade-off between aligning the paths with principal directions and keeping constant path intervals, since most external loading induced principal directions are irregularly distributed with non-zero divergence and rotation. Previous path planning methods using either local or global optimization were theoretically unable to satisfy both requirements due to this contradiction.

In this study, we dealt with this trade-off by introducing a region- based path planning strategy using image representation. Unlike the geometric algorithms used in previous methods which required ad hoc treatments for region partitioning and path planning, for the first time we used image processing algorithms [14] which offered more efficient, robust and unified operations to tackle geometric problems. By taking advantage of image processing techniques, the target region can be robustly decomposed into sub-regions, each of which contains a relatively regular stress distribution and thus can be filled with evenly spaced filaments. In this way, both the alignment and deposition quality can be greatly improved, resulting in strengthened printed parts. The proposed method can also be used in the iterative design process to optimize the functional performance of 3D printed parts under different loading conditions, by aligning the path with principal directions, e.g. from the principal stress, that can supposedly enhance the load-bearing capacities.

2. Problem definition and overview of the proposed method

According to previously reported findings, the better alignment between the filament and the principal direction, the greater overall strength of the 3D printed part. In this study, we set out to deliver the optimized printing paths for the filament fabrication of an input part model M under given static boundary/loading conditions (Figure 1(a)). Since most filament fabrication is in a layer-by-layer fashion, an ordinary finite element analysis (FEA) can be conducted to compute the stress distribution $\sigma(\boldsymbol{x} \in M)$ as a second order tensor field over each layer of the model (Figure 1(b)). The optimization goal is to construct a scalar field $G(\boldsymbol{x} \in M)$ according to σ , such that the summed Rayleigh Quotient $\sum \boldsymbol{x}$ (∇GT σ∇G)/(∇GT ∇G) is globally minimized, while the magnitude of gradient ‖∇G‖ remains constant. In this way, the isocurves of G are believed to best align with the principal direction of σ and remain constant intervals, thus can be treated as the printing paths.

Unfortunately, there is theoretically no deterministic solution to this problem due to the trade-off described earlier. Previous studies attempted to convert this problem into a quadratic optimization problem and obtained fair results for cases with simple stress distribution.

However, a practical stress distribution under a general loading condition might contain degenerated points which potentially jeopardize the optimality using the quadratic solution. Therefore, we proposed to deal with this issue by divide-and-conquer strategy. Unlike other related studies using geometric local searching algorithms to partition tensor and vector fields [15, 16], the input model and its principal directions were converted into image representations (Figure 1 (C)), which reflect the global nature of principal directions and thus allow the partitioning of the principal directional field by robust image processing algorithms. Each sub-region is guaranteed to contain quasi-regular principal directions with near zero divergence and constant rotation, which can be aligned with a group of curves of constant intervals as the printing paths (Figure 1(d)).

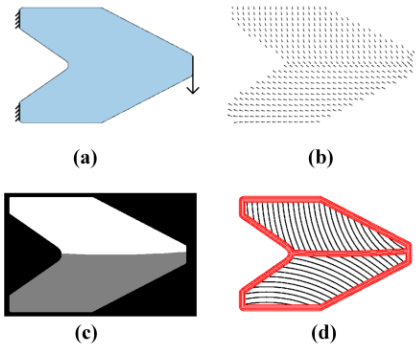

Figure 1. Stress-oriented printing path generation: (a) given model and its loading condition; (b) its principal directions; (c) image partitioning; (d) stress aligned path generation in each sub-region.

3. Grayscale image based stress-oriented printing path generation

3.1 Principal directional field representation

Given an input finite element model M and its principal directions $\sigma(\boldsymbol{x} \in M)$ upon certain loading condition as shown in Figure 1(a) and (b), we can rasterize the model into an image domain I and calculate the principal stress $\boldsymbol{p} = (px, py)$ for $\boldsymbol{i},\boldsymbol{j}$ i,j each pixel Ii,j locating inside M. Those pixels outside M is simply assigned nil value to legalize the representation. This rasterization enables to utilize a variety of unified image processing techniques to deal with this geometric problem in a more robust and efficient manner. To characterize the rasterized principal directions, which is technically a vector field over M, we numerically compute the divergence for each Ii,j via Eq. (1).

$$D = px * Sx + py * Sy \quad (1)$$

where Sx=[−2 0 2] and Sy=[0 0 0] are the
−1 0 1 1 2 1
directional Sobel kernel to calculate the derivatives of the original image. The divergence delineates the uniformity of the vector field, where an irregular region exhibits greater divergence and thus need to be divided. In addition, the value of rotation is computed as a supplement characterization to indicate the circulation change of the vector field, which is also an important criterion for partitioning.

$$R = py * Sx - px * Sy \quad (2)$$

Figure 2 shows the computed image representations of induced divergence (Figure 2 (a)) and rotation of the vector field (Figure 2 (b)), which are normalized into visualized grayscale range. Although not very clear visually, the change in grayscale already delineates the rough boundary of the vector field, which will be later extracted for partitioning the field.

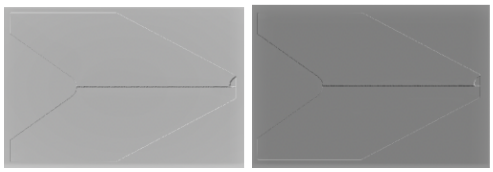

(a) (b)

Figure 2. Image representation of the vector field: (a) computed divergence and (b) rotation value according to Eq. (1) and (2).

3.2 Vector field partitioning

The criterion to partition the vector field is to make sure each sub-region contains no divergence and stable rotation value, which dictates the alignment of principal directions with printing paths with constant intervals. Therefore, we rasterize the computation results of divergence and rotation into grayscale image respectively, as shown in Figure 3. Noticeably, pixels with abrupt change in values already form subtle boundaries to segment the image. Inspired by this observation, we apply boundary detection algorithm to extract those critical pixels from divergence and rotation image, and merge them to produce the critical boundary image.

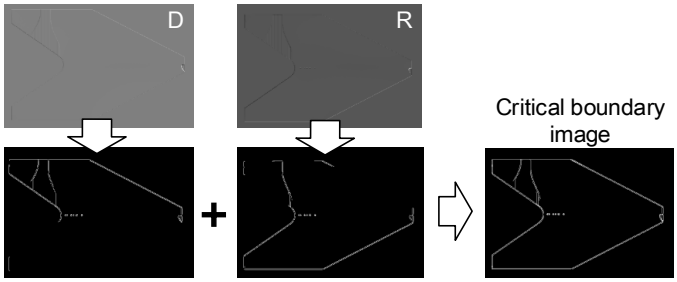

Figure 3. Critical boundary extraction

However, the extracted critical boundary image still contains some outlier pixels that should be eliminated. Additionally, the boundary should avoid areas with stress concentration. In this case, standard image morphological operations are further applied to the critical boundary image to refine the boundary. By applying the dilation and thinning algorithms, the boundaries to partition the image can be successfully extracted, as shown in Figure 3(d). Accordingly, the rasterized vector field is simultaneously partitioned into two sub-regions as depicted in Figure 1(c). The next task is to generate printing paths that best align with the stress distribution for each region.

3.3. Grayscale image based path generation method

In order to maximize the alignment between the filament and the principal directional field, for each sub-region, a group of paths with constant intervals need to be generated with respect to the principal directions. In image domain, this problem is converted into generating a grayscale image such that the iso-grayscale curves of the image directly form the printing paths for each sub- region, as shown in Figure 4(b) and (c). To guarantee that the induced iso-grayscale curves maintain constant interval, the grayscale image should be a Euclidean distance transformation from a seed point as shown in Figure 4(a). Therefore, the generation of such grayscale image is converted into a problem of finding a seed point $\boldsymbol{ps}$, whose connecting line with every pixel $\boldsymbol{Ii,j}$ in the sub-region should be as perpendicular to the principal stress $\boldsymbol{pi,j}$ as possible. Mathematically, the problem is defined as:

$$\boldsymbol{p_s} = argmin\left(\sum_{\boldsymbol{I_{i,j}}} \frac{(\boldsymbol{p_s}-\boldsymbol{I_{i,j}})\cdot \boldsymbol{p_{i,j}}}{\|\boldsymbol{p_s}-\boldsymbol{I_{i,j}}\|}\right) \quad (3)$$

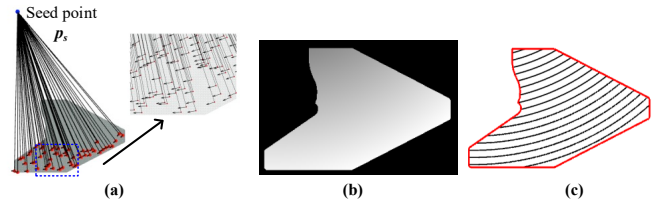

Figure 4. Grayscale image based path generation method: (a) finding seed point; (b) grayscale image generation by Euclidean distance transformation of the seed point; (c) iso-grayscale curve extraction (greater interval is chosen for better visualization).

To find the optimal seed point $\boldsymbol{ps}$, we take advantage of the principle of duality and transform the optimization into a weighted least square problem. As shown in Figure 5, for every pixel $\boldsymbol{Ii,j}$, a line $\boldsymbol{Li,j}$ that passing through $\boldsymbol{Ii,j}$ and perpendicular to $\boldsymbol{pi,j}$ is first computed. The dual of this line, denoted as $\boldsymbol{L*}$, is regarded as a $\boldsymbol{i,j}$ point according to the principle of duality. Therefore, the dual problem is to find the most eligible line $\boldsymbol{Ls}$ passing through all dual points $\boldsymbol{L*}$ with the least weighted square error. Eventually, the $\boldsymbol{i,j}$ dual of this line $\boldsymbol{L*}$ is essentially the desired seed point $\boldsymbol{p}$.

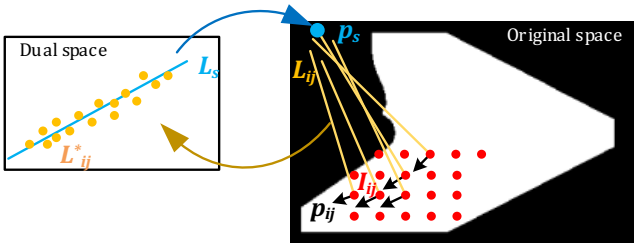

Figure 5. Finding optimal seed point by the principle of duality.

Once the seed point $\boldsymbol{p}$ for each sub-region is computed,
Euclidean distance transform is applied to assign grayscale value for each internal pixel. Specifically, for each pixel $\boldsymbol{Ii,j}$, its grayscale value gi,j is the distance between $\boldsymbol{Ii,j}$ and $\boldsymbol{ps}$. The computation is based on a sequential algorithm [17] which takes only linear time. Results of the generated grayscale image can be seen in Figure 4(b).

3.4 Printing path generation

The aforementioned grayscale image enables to generate stress- oriented printing paths by extracting the iso-grayscale curves for each sub-region. In addition, on the boundary of each sub-region, a few contours of boundary paths should be added to achieve better adhesion between adjacent sub-regions. Thus, the printing paths are created in two-stages. Given an input sub-region and its rasterized stress distribution (Figure 6(a)), we first compute its boundary distance transform image and extract the first three contours of iso-grayscale curves as the boundary paths (Figure 6(b)), which fill up the outmost region. Next, the seed point of the unfilled sub-region is computed as well as its induced distance transform image, which generates iso-grayscale paths to cover the remaining area (Figure 6 (c)). The integration of the two forms are the final printing paths of this sub-region (Figure 6 (d)). Note that the path intervals are chosen according to the size of the printing nozzle and filament. There could be few retraction motions due to the inconsistency of the two forms of paths, therefore, a distance- first algorithm is adopted to link up the paths into a single trajectory with the least number of tool retractions to ensure the fabrication quality. After the printing paths for each sub-region are generated, the combination of them forms the final stress-oriented paths as shown in Figure 1(d).

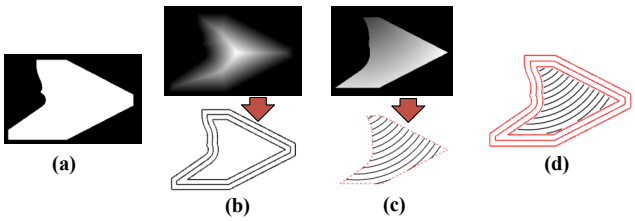

Figure 6. Printing path generation: (a) an input sub-region; (b) boundary distance transform and boundary path; (c) seed point distance transform and stress-oriented path; (d) combined printing path (greater interval is chosen for better visualization).

4. Experimental evaluation

Apart from the above example, 3 more example parts under different loading conditions were selected to demonstrate the effectiveness of the proposed method (see Figure 7). For each part, an ordinary FEA was conducted to compute the principal directional field, which was then transformed into image representation. Critical boundaries of vector fields were extracted to partition them into sub-regions, each of which was filled with boundary paths and stress-oriented paths to reinforce the overall mechanical strength under specified loading conditions. To evaluate the alignment between the printing paths and the principal stress, a discrepancy metric $f = \|\boldsymbol{p}\| \sin\theta$ was i,j $\boldsymbol{i,j}$ defined for each pixel $\boldsymbol{Ii,j}$, where $\boldsymbol{pi,j}$ is the principal stress at $\boldsymbol{Ii,j}$ and θ is the angle between the tangent direction of the printing path and $\boldsymbol{pi,j}$. Figure 8 shows the normalized discrepancy as grayscale image. According to the definition, smaller f indicates i,j smaller grayscale and hence better alignment. Compare with traditional strategies (printing in X direction or Y direction as shown in Figure 8), our stress oriented paths led to darker discrepancy image, and achieved better alignment. Quantitatively, the summation of discrepancy for all pixels was reduced by as much as 70% compared with traditional strategies (printing in either X or Y direction).

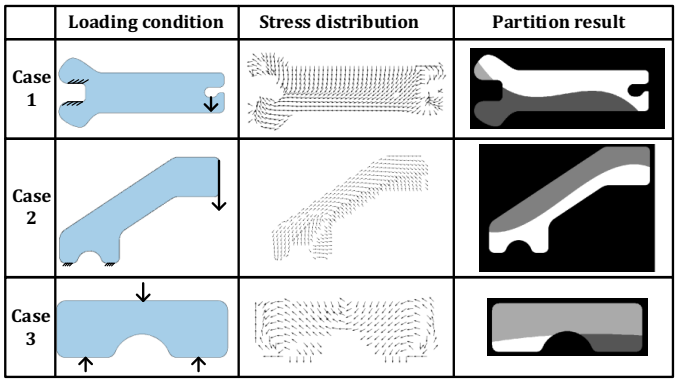

Figure 7. Load-bearing parts under different loading conditions.

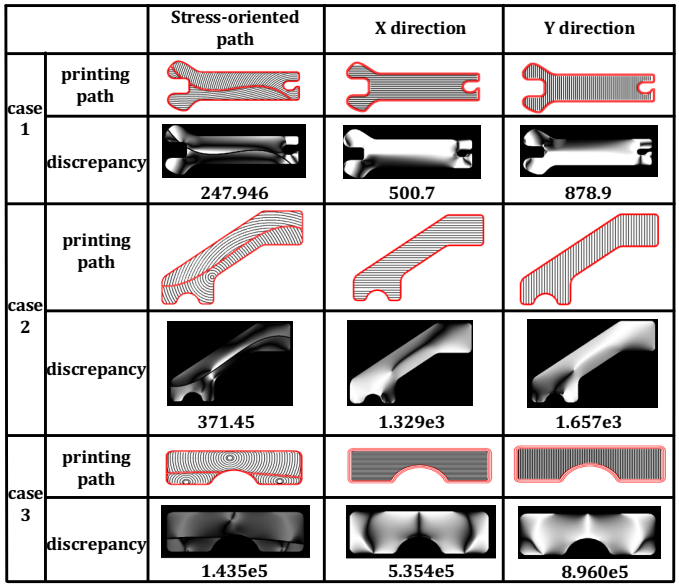

Figure 8. Printing path generated via different strategies and their alignment score.

Three-point bending test was conducted for case 3 (see Figure 9). The testing part was fabricated using the stress-oriented printing path and compared with the one using Ultimaker Cura® , a 3D printing planning software. The strategy by Cura was to use parallel path along ±45 ° direction in alternating sequence over the staking layers to reach a quasi-isotropic strength. Both testing parts were additively made with the same PLA filament and by the same 3D printer and were equally weighted.

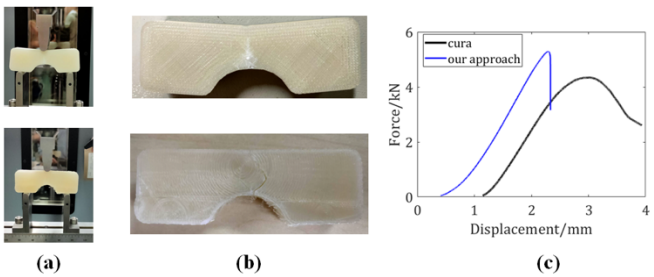

Figure 9. Three-point bending test for case 3: (a) test setup; (b) breaking pattern; (c) tensile strength.

As shown in Figure 9 (c), the tensile strength was increased by approximately 20% for the part fabricated using the stress- oriented printing paths. It was however noticed that such strategy also suffered from a sudden loss of strength when the loading reached the maximum. To cope with such issue, a mixed strategy combining 33% of layers with our printing paths and 67% of layers from Cura was used and tested (see the red curve in Figure 9 (c)). A 15% increase of tensile strength was observed together with a much enhanced ductility to withstand more complex loading conditions. It can be anticipated that, if FRP filament was chosen, much stronger tensile strength could be achieved.

5. Conclusions

The anisotropy of mechanical property observed in filament fabricated parts makes the printing path planning a vital challenge to enhance load-bearing capacity. Desired printing paths are expected to align with the principal directions while maintaining constant path intervals. This research proposed a stress-oriented printing path strategy, and for the first time proved that image processing algorithms can be used to partition the principal directional field and generate printing paths aligned with principal directions. The part fabricated using the optimized printing paths achieved noticeable increase in tensile strength in the test, compared with commercial systems. Further work is to extend the method for more complex loading conditions by layer-wise computation of optimized paths, and to conduct more testing using carbon fibre reinforced plastic filaments.

Acknowledgements

This work was supported by the National Natural Science Foundation of China (Ref: 51805260) and the National Science Fund for Distinguished Young Scholars (Ref: 51925505).

References

[1] Tekinalp, H. L., Kunc, V., Velez-Garcia, G. M., Duty, C. E., Love, L. J., Naskar, A. K., Blue, C. A., and Ozcan, S., 2014, Highly oriented carbon fiber–polymer composites via additive manufacturing, Composites Science and Technology, 105, 144-150
[2] Li, N., Li, Y., and Liu, S., 2016, Rapid prototyping of continuous carbon fiber reinforced polylactic acid composites by 3D printing, Journal of Materials Processing Technology, 238, 218-225
[3] Li, N., Link, G., and Jelonnek, J., 2020, Rapid 3D microwave printing of continuous carbon fiber reinforced plastics, CIRP Annals, 69, 221-224
[4] Riddick, J. C., Haile, M. A., Von Wahlde, R., Cole, D. P., Bamiduro, O., and Johnson, T. E., 2016, Fractographic analysis of tensile failure of acrylonitrile-butadiene-styrene fabricated by fused deposition modeling, Additive Manufacturing, 11, 49-59
[5] Michell, A. G. M., 1904, LVIII. The limits of economy of material in frame-structures, London, Edinburgh & Dublin Philosophical Magazine & Journal of Science, 8, 589-597 [6] Fang, G., Zhang, T., Zhong, S., Chen, X., Zhong, Z., and Wang, C. C., 2020, Reinforced FDM: multi-axis filament alignment with controlled anisotropic strength, ACM Transactions on Graphics (TOG), 39, 1-15
[7] Thompson, M. K., Moroni, G., Vaneker, T., Fadel, G., Campbell, R. I., Gibson, I., Bernard, A., Schulz, J., Graf, P., and Ahuja, B., 2016, Design for Additive Manufacturing:

Trends, opportunities, considerations, and constraints, CIRP annals, 65, 737-760
[8] Vaneker, T., Bernard, A., Moroni, G., Gibson, I., and Zhang, Y., 2020, Design for additive manufacturing: Framework and methodology, CIRP Annals, 69, 578-599
[9] Steuben, J. C., Iliopoulos, A. P., and Michopoulos, J. G., 2016, Implicit slicing for functionally tailored additive manufacturing, Computer-Aided Design, 77, 107-119 [10] Tam, K.-M. M. and Mueller, C. T., 2017, Additive manufacturing along principal stress lines, 3D Printing and Additive Manufacturing, 4, 63-81
[11] Zhang, H., Yang, D., and Sheng, Y., 2018, Performance-driven 3D printing of continuous curved carbon fibre reinforced polymer composites: A preliminary numerical study, Composites Part B: Engineering, 151, 256-264
[12] Wang, T., Li, N., Link, G., Jelonnek, J., Fleischer, J., Dittus, J., and Kupzik, D., Load-dependent path planning method for 3D printing of continuous fiber reinforced plastics, Composites Part A: Applied Science and Manufacturing, 140, 106181
[13] Sun, Y., Tian, W., Zhang, T., Chen, P., and Li, M., 2020, Strength and toughness enhancement in 3d printing via bioinspired toolpath, Materials & Design, 185, 108239 [14] Russ, J. C., "Image processing," in *Computer-assisted microscopy*, 1990, pp. 33-69. [15] Liu, X., Li, Y., Ma, S., and Lee, C.-h., 2015, A tool path generation method for freeform surface machining by introducing the tensor property of machining strip width, Computer-Aided Design, 66, 1-13
[16] Ma, J.-w., Lu, X., Li, G.-l., Qu, Z.-w., and Qin, F.-z., 2020, Toolpath topology design based on vector field of tool feeding direction in sub-regional processing for complex curved surface, Journal of Manufacturing Processes, 52, 44-57
[17] Maurer, C. R., Qi, R., and Raghavan, V., 2003, A linear time algorithm for computing exact Euclidean distance transforms of binary images in arbitrary dimensions, IEEE Transactions on Pattern Analysis and Machine Intelligence, 25, 265-270.